Engineering Failure Analysis 46 (2014) 49–61

Contents lists available at ScienceDirect

Engineering Failure Analysis

journal homepage: www.elsevier.com/locate/engfailanal

Parametric study on damage and load demand of prestressed concrete crosstie and fastening systems

Zhe Chen [a], Moochul Shin [b], Bassem Andrawes [c,*], John Riley Edwards [d]

[a] Department of Civil and Environmental Engineering, University of Illinois at Urbana-Champaign, 205 North Mathews Avenue, Urbana, IL 61801, United States
[b] Department of Civil and Environmental Engineering, Western New England University, 1215 Wilbraham Road, Springfield, MA 01119, United States
[c] Department of Civil and Environmental Engineering, University of Illinois at Urbana-Champaign, 205 North Mathews Avenue, Urbana, IL 61801, United States
[d] Rail Transportation and Engineering Center (RailTEC), Department of Civil and Environmental Engineering, University of Illinois at Urbana-Champaign, 205 North Mathews Avenue, Urbana, IL 61801, United States

ARTICLE INFO

Article history:
Received 2 May 2014
Received in revised form 2 August 2014
Accepted 6 August 2014
Available online 14 August 2014

Keywords:
Prestressed concrete crosstie
Railway superstructure
Fastening systems
Finite element modeling
Failure mechanisms

ABSTRACT

There is an increasing interest in the performance and serviceability of concrete crossties and elastic fastening systems due to the loading demands of increasing freight axle loads and the development of new high-speed passenger rail infrastructure in North America. In the light of these increasing demands, it is essential to examine and improve current design practices of prestressed concrete crossties and fastening systems. This study focuses on developing an analytical framework for a 3D finite element (FE) model of prestressed concrete crossties and fastening systems to improve the knowledge regarding its mechanical behavior. Parametric studies are conducted based on the detailed FE model to analyse the damage and load demands associated with two major failure mechanisms in concrete crosstie and fastening system, namely the tensile-cracking failure of concrete crosstie and the damage of fastening system. The following parameters are considered in the studies: bond-slip behavior between concrete and prestressing strand, support conditions of concrete crosstie, material properties of rail pad assembly, and wheel load position. The parametric studies presented the detailed stress state of the failure mechanisms and the thresholds for performance.

© 2014 Elsevier Ltd. All rights reserved.

1. Introduction

With the development of high-speed rail corridors and ever increasing axle loads in North America, there is increasing demand on the railroad infrastructure and its components. The dominant design approach for the concrete crosstie and fastening system still remains primarily empirical. This is evident by the fact that the relation using speed and traffic to determine the design load in American Railroad Engineering and Maintenance-of-way Association (AREMA)'s Recommended Practices has been developed empirically [1]. To ensure that freight and passengers are transported safely, components remain in track for their intended service life, and that proper track geometry is maintained, further investigation into the behavior and interaction of the concrete crosstie and fastening systems is needed. In addition, a mechanistic design approach based on detailed structural analysis would be beneficial for infrastructure manufacturers to reduce costs on over-designed components and efficiently to improve the designs of the components to next generation.

* Corresponding author.
E-mail address: andrawes@illinois.edu (B. Andrawes).

http://dx.doi.org/10.1016/j.engfailanal.2014.08.002
1350-6307/© 2014 Elsevier Ltd. All rights reserved.

To date, few models have been developed to address the mechanistic design and performance of concrete crossties and fastening systems. González-Nicieza et al. [2] have developed a failure analysis of a railway track used for transporting heavy-haul industrial freight. Based on data collected from field investigation, single-crosstie model and multiple-crosstie model have been built to look into the cause of crosstie cracking. However the model assumed elastic material property for all the track components, and the fastening system was ignored. Rezaie et al. [3] also used an FE model to investigate the cause for longitudinal cracks in concrete crossties. Nonlinear material property was defined in the model, but the study mainly focused on the concrete crosstie response under increasing shoulder insert pressure. Some mathematical and FE models have been developed to investigate the dynamic interaction between the vehicle and the track structure. Frohling [4] proposed a mathematical model to predict the track deterioration due to dynamic wheel loading and spatially varying track stiffness. Kaewunruen and Remennikov [5] also presented a dynamic FE model of the concrete crosstie to investigate its dynamic response. The model only included the concrete crosstie and all other components were replaced with springs. In addition, many analytical/numerical studies have focused on the behaviors of the systems under the vertical wheel loading. Among those, Yu and Jeong [6] presented a 3D finite element model including a prestressed concrete crosstie and ballast. Prestress and direct uniaxial, static rail-seat loading were considered in the model. A quarter-symmetric model was used to compare the performance of the concrete crosstie on different support conditions. One of the model's limitations was assuming full bond between the concrete and strand, hence ignoring the possibility of relative slip of strands causing the effect of prestress to be magnified. Yu et al. [7] presented an improved finite element model of the concrete crosstie with ballast and subgrade support. In this model, the interaction between concrete and strands was modeled as cohesive element, and the cohesive element was incorporated between concrete and strands to simulate a linear bond-slip relationship. Dahlberg and Lundqivst [8] investigated the effects of different support conditions on the rail track systems using a 3D finite element model. They concluded that the higher vertical force would be transmitted to adjacent concrete crosstie as the loaded crosstie was poorly supported. In conclusion, using currently available models to assess the mechanical behaviors, especially interactions of each component of the prestressed concrete crossties and fastening systems is not feasible since the models consisted of only some of the components. Therefore, this study focuses on developing an FE model of a prestressed concrete crosstie with detailed fastening system components that can be a tool to explore the mechanical interactions and behaviors of the crosstie and fastening systems. Nonlinear material properties are defined for all the components, and the model considers the effect of vertical loading, lateral loading and concrete prestress. Fig. 1 shows a schematic of a prestressed concrete crosstie with fastening system on ballast (a) and a typical fastening system that consists of clips, cast-in shoulders, insulators and rail pads (b). With the developed FE model, parametric studies are conducted to investigate the two major failure mechanisms of the concrete crosstie and fastening system, namely, the damage of the fastening system and the tensile cracking of concrete crosstie.

1.1. Current design practice

As an element of the track structure, a crosstie is designed to transmit vertical, lateral and longitudinal forces to ballast and subgrade while supporting rails and fastening systems. This study specifically focuses on the prestressed concrete crosstie since it has replaced timber crossties in certain applications and has been installed in field for last several decades [9]. Based on experimental studies and numerical models, some understanding about the behavior of the track structure has been established. For example, the AREMA manual, Australian Standard, and UIC design standard [1,10,11] have all recommended different methodologies to quantify the flexural demand of concrete crosstie. However, some of the failure mechanisms, including center binding and rail seat concrete damage due to insufficient prestress, are not explicitly considered in the current standard. Using the detailed FE model, one objective of this study is to investigate the component demand and component interaction that is related to the failure mechanism of the concrete crosstie and fastening system.

Fastening systems, which are designed to behave elastically given the nature of the materials used to construct them, are placed to fasten rails to crossties. The main functionalities of the fastening system include gauge restraint, transferring the

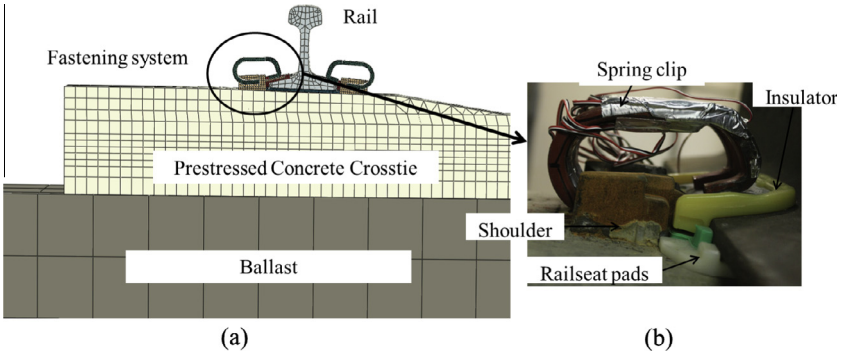

Fig. 1. Schematic of a prestressed concrete crosstie and fastening system (a) and a typical fastening system (b).

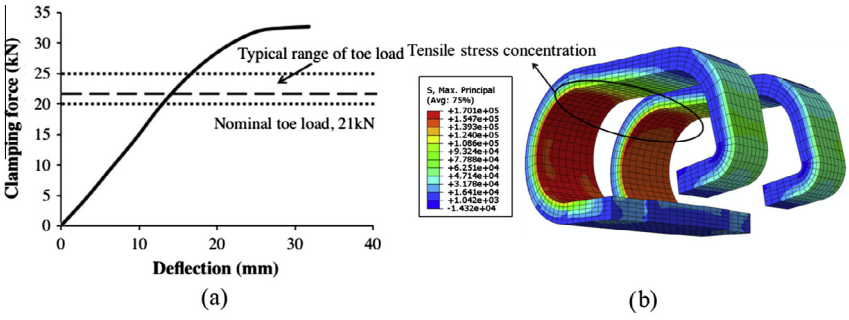

Fig. 2. (a) Typical clamping force and deflection curve. (b) Tensile stress concentration on the rail clip (unit: psi, 1 psi = 0.007 MPa).

vertical, lateral and longitudinal loads from rails to crossties, load/impact attenuation, electrical isolation and providing rail seat cant [1]. The fastening system should be adequately designed and manufactured such that the track system would be functional under all anticipated loading and environmental conditions. In the current AREMA Manual, some evaluative tests are specified to ensure the quality of the fastening system, but a comprehensive design methodology is still missing.

Fig. 2.a shows the rail-seat clamping force and deflection curve of the elastic fastening system in this study. Most of current elastic fastening systems are designed to apply about 21 kN (4710 lb) of nominal clamping force to the rail system. Since two clips are installed on one rail seat (see Fig. 1b), 10.5 kN (2355 lb) of clamping force is applied by one clip. Furthermore, a typical range of the clamping force is between 20 kN (4400 lb) to 25 kN (5600 lb). If the clamping force is less than a certain ratio of the load, the clamping force is insufficient to hold the rail, but if the clamping force is greater than a certain threshold, it indicates that the clip experience severe yielding. The output of FE model revealed that under large clamping force, the rail clip is likely to yield in tension at some region, as shown in Fig. 2b). The safe working range of the clamping force from one clip is determined as 10.5 kN ± 1300 N (300 lb).

1.2. Research necessity based on international survey

The Rail Transportation and Engineering Center (RailTEC) at the University of Illinois at Urbana-Champaign (UIUC) conducted a survey on the international railway industry's state of practice regarding the concrete crossties and fastening systems design, performance and research needs [12]. The results from the survey highlighted the most common failure mechanisms of the concrete crossties and fastening systems. Fig. 3 shows the survey results on the most critical problems related to concrete crossties and fastening systems. The survey was ranked from 1 to 8 with 8 being the most critical. The international response and domestic responses (North America) were quite different in terms of the most prominent failure modes. In North America, the most common failure modes are rail seat deterioration (RSD), and fastening system wear and damage. Outside of North America, tamping damage is the most critical failure mode as well as the fastening system wear and damage. Additionally, concrete crosstie failure due to cracking has drawn the attention of both. The cracking of concrete crosstie due to center binding is acknowledged as a high-risk failure mechanism both internationally and in North America.

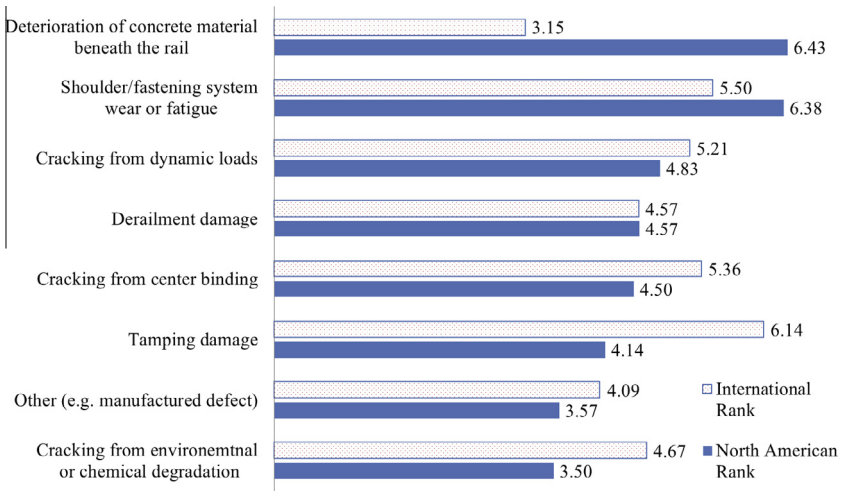

Fig. 3. The most critical concrete crosstie and fastening system problems [12].

Based on the research necessity, in this paper a detailed 3D concrete crosstie and fastening system model was developed and analyzed using the finite element program ABAQUS [13] under various loading scenarios including prestress force, vertical wheel loading and lateral wheel loading at different ratios.

2. Finite element model configuration

In order to examine the responses of the fastening system under different loading scenarios, and to determine the center binding mechanism of concrete crosstie, a 3D FE model that includes two sets of fastening systems on a single concrete crosstie and simplified supports was developed. The clip model was validated previously with the clamping force–deflection relationship provided from the manufacturer [14]. The FE system model is validated with laboratory and field experiment conducted at the University of Illinois at Urbana-Champaign [15]. As the model validation is outside the scope of this discussion, it is not described in detail.

Fig. 4 illustrates the layout of the fastening system in the FE model. As shown, the fastening system is fixed to the concrete crosstie to transmit loading from the rail to the concrete surface and maintain uniform track geometry. The fastening system modeled in this paper includes embedded iron shoulders, clips, nylon insulators, and a rail-seat pads system consisting of a resilient polyurethane pad for load attenuation and a nylon abrasion plate to mitigate abrasion of the concrete. The embedded shoulder provides support for other components. The clip is deformed initially and inserted into the shoulder to prevent longitudinal and lateral displacement of the rail. The insulator is placed between the clip and the rail to provide electrical isolation between the two rails to ensure the signal system is not shunted. In the working environment, the wheel loading can be divided into a vertical load, which is applied on the top of the head of the rail, and a lateral load, which is applied at edge of the head of the rail. In this model the geometries of all the components were simplified based on manufacturer design to improve calculation efficiency.

The whole track structure is included in the model to evaluate the system response under the asymmetric loading scenario on curved track. The design of concrete crosstie and fastening system modeled in this study is widely installed on heavy freight track in North America. The dimension of the crosstie is 2.59 m (102 in.) (length) × 0.28 m (11 in.) (width) × 0.24 m (9.5 in.) (height) with 20 embedded prestressing strands. The section area of the prestressing strand is 22 mm^2 (0.034 $in.^2$), and the distribution of prestressing strands in the concrete crosstie is shown in Fig. 4.

The modeling work was carried out using ABAQUS Standard. The rail, fastening system, concrete crosstie and supporting ballast were all modeled with eight-node brick element that has three translational degrees of freedom (DOF) at each node, and the prestressing reinforcement was modelled with 1-D truss element that only had stiffness along the longitudinal direction. Based on the geometry of the components, different mesh densities were assigned to different components based on the result of mesh sensitivity analysis. For the clip, as large deformation occurred and the component response was sensitive to mesh density when applying clamping forces, dense mesh was assigned; and as the ballast only served as the general representation of the track substructure, it was coarsely meshed. Fig. 4 shows the relative density of mesh.

2.1. Constitutive relationships

Concrete damaged plasticity model was used to define the concrete material property. In this material model, two main failure mechanisms were considered, namely, tensile cracking and compressive crushing. Under uniaxial tension, concrete first goes through a linear-elastic stage, and when stress reaches cracking stress it follows a softening stress–strain

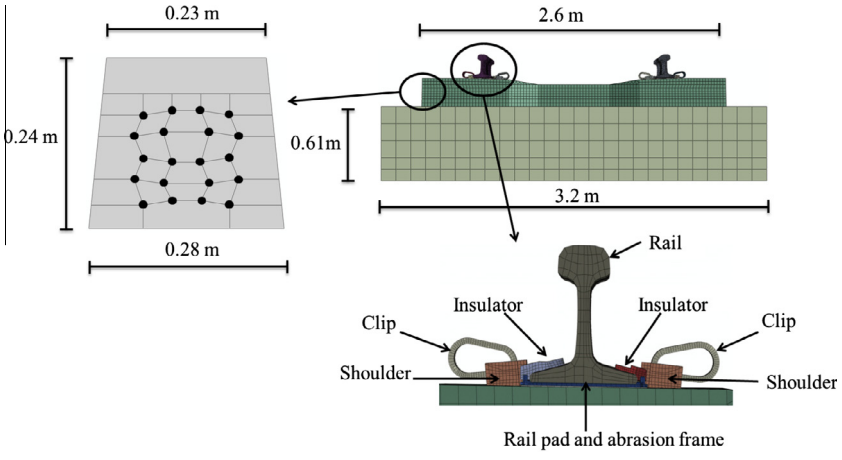

Fig. 4. Configuration of the 3D concrete crosstie and fastening system model.

Table 1
Material properties of model components considered in the study.

Component	Young's modulus (MPa)			Poisson's ratio	Yielding strength (MPa)	Ultimate/peak strength (MPa)	Cracking strength (MPa)
Concrete	29,970			0.2	NA	48	5
Clip	158,585			0.29	1261	1393	
Shoulder	168,928			0.3	1,261,310	448	
Strand	223,274			0.3	1758	1758	
Rail	206,850			0.3	1034	1034	
	RPS1	RPS2	RPS3				
Insulator	7520	2507	2507	0.39	64	84	
Rail pad	2379	792	238	0.49	8	35	
Abrasion plate	7520	2507	2507	0.39	64	84	

relationship. Under uniaxial compression the initial response is linear until the yielding stress is reached. In the plastic stage, the response is first characterized by strain hardening and then strain softening after reaching its compressive peak stress. As cyclic loading is not included in the current model, damage parameters related to stiffness reduction in the unloading process are not defined.

For all the components of the fastening system including shoulder, clip, rail pad, abrasion plate, insulator as well as rail, a two-stage material property model was assigned. In the beginning it follows an elastic relationship, and the plastic stage consists of a strain-hardening range followed by a strain-softening range. Critical parameters used in the definitions of the constitutive relationships for fastening system components are summarized in Table 1. Herein, wide range of the elastic modulus of pad and plate were considered and parametric studies were carried out with three different rail-seat pad systems, since the material properties of the pad systems greatly vary depending on temperature, manufacturing process, composite materials, etc. The nomenclature of the different rail-seat pad systems (RPS1, RPS2, and RPS3) and their elastic modulus selected in the following parametric study on the fastening system are also summarized in Table 1.

To provide a realistic support for the concrete crosstie, a ballast section of 0.61 m (24 in.) depth was also included in the model. However, the modeling of track substructure itself was quite intricate as it consisted of multiple layers of granites and soil (ballast, subballast, subgrade, etc.) of inhomogeneous material property. Discrete element method (DEM) provides an alternative to accurately capture the response of a track substructure and relevant research work has already been published [16]. However, the DEM simulation is often computationally expensive. As the emphasis of this research work lies in the modeling of concrete crosstie and fastening system, the ballast model herein mainly served as a general representation of the track substructure, and the material property was defined based on the track stiffness (vertical load increment divided by vertical deflection increment of concrete crosstie) measured in Transportation Technology Center Inc. at Pueblo, CO. [17]. In the field test, the vertical deflection of concrete crosstie was measured under monotonic static vertical load, and it was observed that the track stiffness considerably increased at higher vertical wheel load. To capture this nonlinear behavior, the hyperelastic material model was used for ballast, in which the stress–strain relationship can be calibrated point-by-point according to the result of field experimentation.

2.2. Component interaction

Interaction between different components of the fastening system was defined with contact pairs in ABAQUS [13]. A master surface and a slave surface of different mesh densities were identified. Some of the coefficient of friction (CoF) values were based on a series of large-scale abrasion resistance tests that were conducted recently at the University of Illinois at Urbana-Champaign (UIUC) [18], and others are determined based on empirical data [19,20].

The interaction between the concrete crosstie and shoulder inserts was relatively complex as it involves multiple pairs of surface interaction. To avoid numerical singularity and to simplify the mesh of concrete, "embedded region" in ABAQUS was used to model the interaction. With this constraint, the translational DOF of the embedded element (shoulder element) is restrained by the corresponding DOF of the host element (concrete element). And with "embedded region" the bond characteristics between concrete and shoulder insert can be reasonably represented until damage occurs.

Based on the manufacturer design, the gap between an insulator and shoulder could not be explicitly determined, since the degree of the uncertainties of the gap is significant. In the 3D model, the gap was set to be 0.05 mm (0.002 in.), as a relative sliding between concrete and abrasion plate has been often observed in a laboratory setting. This is important because the interaction between the shoulder and insulator considerably affects the load path through the fastening system under lateral load. Due to this gap, under lateral wheel load lateral resistance first comes from the friction between the abrasion plate and concrete, and the uneven clamping force due to rail sliding. As the insulator and shoulder comes in contact, the lateral resistance from the shoulder shares some portion of the lateral load.

Connector element was used to define the interaction between the concrete and prestressed strands. Concrete was meshed in a way that element nodes along the line of the strands coincided with strand nodes and a connector element connected coincident concrete and strand nodes. Cartesian connector section was assigned to the connector element, and the connector element acted as a spring based on the relative displacements of the connected nodes. For simplification the

bond-slip behavior is averaged over the length of reinforcement, and an elastic force–displacement relationship was defined for all the connectors. The stiffness along the direction of the strands was defined based on the pull-out test results of identical materials [21], and it was determined as 137,888 kN/m/m (20000 lb/in/in) (spring stiffness over unit length of the reinforcement). The stiffness will be varied later in the parametric study to investigate its effect on the release of prestress. In addition, nearly rigid connection was defined in the other two directions of connector elements.

2.3. Boundary conditions and loadings

In total, seven static analysis steps were carried out. The loading sequence is as shown in Fig. 5. At the beginning of analysis, based on manufacturer design a total prestress force of 623 kN (140 kips) was assigned to the 20 strands, which is 80% of the total tensile capacity of the strands, and prestress was released in the first step. At the same time, clips were lifted with pressure loading while the clip base was restrained with separate boundary conditions. This is to prepare the clips for further installation. In the second step, clips were inserted into shoulders with displacement boundary condition and clip toes started to be in contact with insulators applying clamping force to the system. In the following three steps, stabilizing boundary conditions and loadings were gradually removed from the model, and at the end of the fifth step the model was ready for loading. At this time the only boundary condition applied was at the bottom of ballast to provide support to the system. Identical vertical loading was applied at the top of the two rails as surface traction in the sixth step, and the loading linearly increased to the maximum value. While the vertical loading remained constant in the seventh step, the lateral loading was applied on the lateral surface of one rail, which is assumed as the high rail in a curve, and linearly increased to the target value. The loading magnitude and position varies according to design loading scenarios and is elaborated in the corresponding subsection.

3. Study on the factors related to tensile cracking of concrete crosstie

3.1. Prestress and bond-slip behavior

The bond-slip behavior between concrete and strands is crucial to the performance of the prestressed concrete crosstie as it determines the initial stress state of concrete before any loading. To investigate the effect of the bond-slip behavior between concrete and reinforcement on the prestress state of concrete crosstie, a component model of concrete crosstie was built. The component model was the same as described above, and only one loading step was defined, which included the release of prestress. As mentioned before the bond-slip behavior was simplified and an elastic force–displacement relationship was defined for the connectors. The elastic stiffness of connectors served as the varying parameter in this parametric study. Based on some available pull-out test results in literature [22–25], four elastic stiffness values were chosen for this parametric study including 137,888 kN/m/m (20000 lb/in/in), 275,777 kN/m/m (40,000 lb/in/in), 413,665 kN/m/m (60,000 lb/in/in) and 551,553 kN/m/m (80,000 lb/in/in). The four cases were generated to represent a realistic range of possible bond-slip behavior in prestressed concrete crosstie.

During release of the concrete crosstie, one critical parameter is the transfer length, which is defined as the length from the end of the strand to the point where the effective stress is developed. In the field, the wheel loading is applied at the two

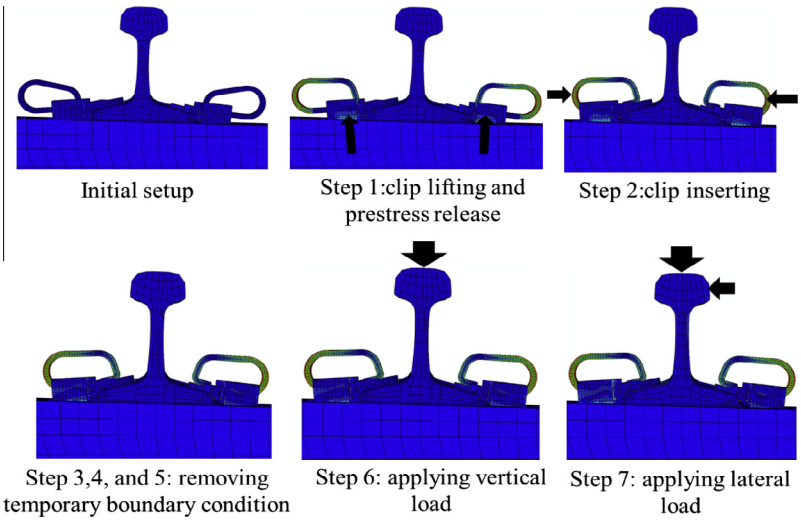

Fig. 5. Loading sequence of the model.

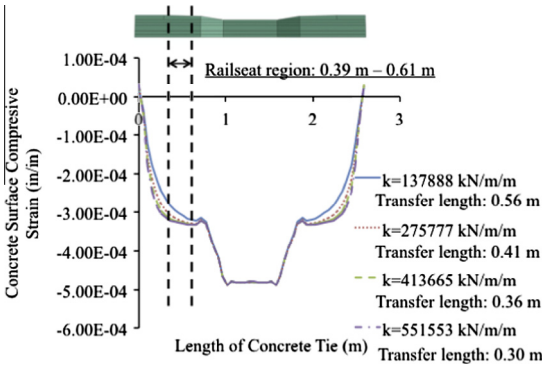

Fig. 6. Concrete surface strain distribution along the length of concrete crosstie.

rail-seat regions, and it would be desirable to have fully transferred prestress in the rail-seat regions. As the four cases represent the range of possible bond-slip behavior in prestressed concrete crosstie, the output of the four cases were used to evaluate the range of transfer length of existing prestressed concrete crossties. The transfer lengths of the four models are summarized in Fig. 6. The transfer lengths were determined based on the concrete surface compressive strain in the longitudinal direction at the centroid height of prestressing strands using 95% Average Maximum Strain (AMS) method, as shown in Fig. 6.

Considering the end of concrete crosstie as the origin point, the distance of the rail-seat region of the concrete crosstie falls between 0.39 m (15.4 in.) and 0.61 m (24 in.). In 2012, Murphy and Peterman presented the transfer length measurement of 220 prestressed concrete crossties. The crossties were provided by four major manufacturers of concrete crosstie in North America [26]. In comparison, the transfer length of the cases generated in this parametric study is within the range of the laboratory measurement. In the two cases where the bond-slip stiffness was defined as 137,888 kN/m/m (20,000 lb/in./in.) and 275,777 kN/m/m (40,000 lb/in./in.), the rail-seat region was partially included in the transfer-length region; and in the other two cases where higher bond-slip stiffness was defined, the transfer length was shorter than 0.39 m (15.4 in.) and the concrete prestress was fully transferred in the rail-seat region. When the elastic stiffness of connectors increased from 137,888 kN/m/m (20,000 lb/in./in.) to 275,777 kN/m/m (40,000 lb/in./in.), the transfer length reduced from 0.56 m (22 in.) to 0.41 m (16 in.). However, when the elastic stiffness of connectors was relatively high, further increase in the elastic stiffness only resulted in a small reduction in transfer length. In summary, the case with bond-slip stiffness of 275,777 kN/m/m (40,000 lb/in./in.) is the threshold for desirable transfer length, and the any weaker bond between concrete and prestressing reinforcement results in insufficient prestress in the rail-seat region. The threshold can also be expressed as 16,501 MPa/m (60.6 ksi/in.), which is the equivalent pullout stress divided by reinforcement end slip.

3.2. Center binding

The cracking of concrete crosstie due to center binding has been identified as one of the critical problems that result in the failure of the concrete crosstie and fastening system. The mechanism for center binding begins as the support of ballast under the crosstie is initially concentrated at the rail-seat rather than uniformly distributed [27]. Over time as the cyclic loading of the vehicles is applied, the depression and abrasion of the ballast is most severe under the rail-seat area of the crosstie. As a result, firm support of the ballast is only provided at the center of the crosstie, and the crosstie cantilevers over its two ends. Under the new support condition, when wheel loading is applied, large negative moment exists at the midspan and results in tensile cracking at the top surface. Fig. 7 shows an example of the tensile cracks due to center binding in concrete crossties.

To simulate the support condition that causes center binding, the geometry of the ballast was changed according to the field observation described in Ref. [27]. Firm support was provided at the midspan of the crosstie, and two slopes were placed close to the rail seat, which allowed a gap between the concrete crosstie and the ballast at the rail-seat area. Based on the model deflection of concrete crosstie and literatures regarding the depression of the ballast [16], four models with firm support (i.e. no gap), 1.27 mm (0.05 in.) gap, 2.54 mm (0.1 in.) gap, and 3.81 mm (0.15 in.) gap were built and compared in terms of the concrete crosstie response. The FE model with exaggerated gaps under rail-seat regions is shown in Fig. 8. A vertical loading of 267 kN (60 kips) was applied in increments to both rail-seats, and a lateral loading of 133.5 kN (30 kips) was applied to one rail-seat to simulate the loading scenario of curved track. The loading scenario was determined based on the load environment specified in AREMA Chapter 30 for mainline freight traffic in North America.

To evaluate the effect of support conditions on the behavior of crosstie, the relationship between the vertical load and midspan concrete flexural stress was generated and shown in Fig. 9. Due to prestress release, a compressive stress of 16.7 MPa (2421 psi) was applied at the top surface of crosstie midspan. When there was no gap between the crosstie and the ballast, the crosstie performed as a beam on elastic foundation. The top-surface concrete flexural stress at midspan

Fig. 7. Cracked concrete crosstie due to center binding.

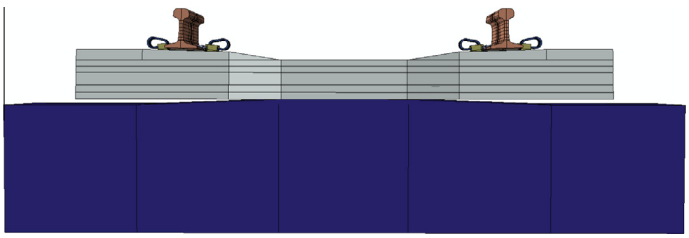

Fig. 8. Layout of the FE model with exaggerated gap under rail-seat regions.

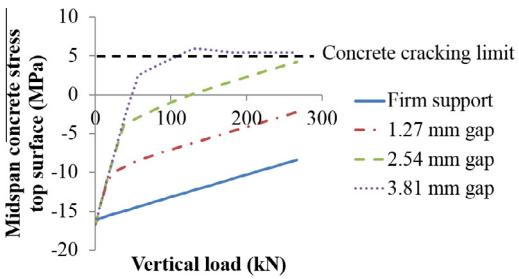

Fig. 9. Relationship between vertical loading and concrete crosstie midspan tensile stress.

gradually decreased and remained compressive under the full vertical load. However, when there was initial gap before loading, the crosstie performed as a beam that was firmly supported at the midspan and cantilevered over the two ends. The midspan concrete flexural stress on the top surface rapidly increased until the bottom of concrete was in contact with the ballast. With a gap of 3.81 mm (0.15 in.), the identical load resulted in tensile cracking at the midspan of concrete crosstie. At the same time, the maximum compressive stress of concrete took place at the shoulder insert, as shown in Fig. 10.

In this parametric study, it can be observed that gaps between concrete crossties and ballast at the rail-seat region considerably increased the flexural demand at crosstie center. For the type of prestressed concrete crosstie in this study, a gap of 2.54 mm (0.1 in.) is the threshold for allowable gap size, and any larger gap between the crosstie and ballast at the rail-seat region will result in tensile cracking at crosstie midspan. Although center binding rises as a structural problem in concrete crosstie, a possible solution to the problem is more related to the ballast surface profile than to the design of the concrete crosstie. Regular track surfacing work including tamping, stoneblowing, or undercutting eliminates gaps between concrete crosstie and ballast, and provide desirable uniform support condition for the crosstie [27].

4. Study on the factors related to the damage of fastening system

In this section, damage of the fastening system was investigated in terms of changes of the clamping force under different loading scenarios, and lateral load demands on field-side shoulder using the described FE model.

A wheel load can be divided into a lateral and a vertical load. Due to the conical shape of the wheel, the load is usually applied at the top of the rail in the gage side (see VG in Fig. 11). However, due to the hunting and/or the hollow-worn wheel,

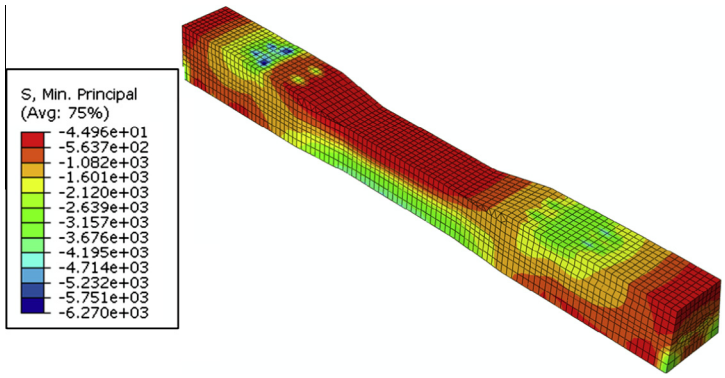

Fig. 10. Compressive stress contour of loaded concrete crosstie with 3.81 mm (0.15 in.) gap between concrete crosstie and ballast (unit: psi, 1 psi = 0.007 MPa).

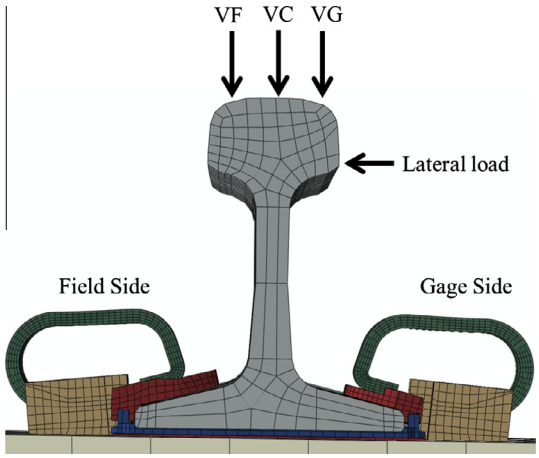

Fig. 11. Three different possible locations of vertical loading.

the load can be shifted to the field side or the center of the rail [28]. Fig. 11 shows the three different locations of the vertical loads considered in the study and the lateral load. VF indicates the vertical load applied at the field side of the rail, VC indicates the vertical load applied at the center of the rail, and the VG indicates the vertical load applied at the gage side of the rail. After vertical load was applied, lateral load was applied at the gauge side of the rail head.

Wheel loadings of different vehicles, speeds, and track degrees of the curves are provided in the AREMA manual chapter 30 [1]. According to the manual, the maximum vertical load is 533 kN (120 kips). It is well known that the single vertical load would be transmitted to several adjacent crossties. When the spacing of the concrete crosstie is 0.61 m (24 in.), based on the vertical load distribution recommended for concrete crosstie in AREMA Manual, 50% of the vertical load would be transmitted into one single crosstie [1]. Therefore, in this study vertical loads of 67, 133, 200, and 267 kN (15, 30, 45 and 60 kips) were applied at the three different locations to cover a wide range of loading scenarios with different spacing, speed, curve conditions and different support conditions underneath each crosstie. The lateral load gradually increased while the vertical load remained constant until the fastening system failed as it was designed.

4.1. Damage in the clips

To prevent the plastic deformation in the rail clip, based on the FE analysis the adopted failure criterion of the fastening system is that the change of the clamping force should be less than ±1300 N (300 lb). A total of 12 simulations (three locations of the vertical force × four different magnitudes of the vertical load) were carried out to examine the effects of vertical load location and magnitude on the changes of the clamping force in the clips. The rail-seat pad system 1 (RPS1) was used for all 12 simulations (see Table 1).

Fig. 12 demonstrates the relationship between the changes of the clamping force with respect to the L/V ratio for the simulation cases, when a vertical load of 200 kN (45 kip) was applied at the gage side (V200G), at the center (V200C), and at the

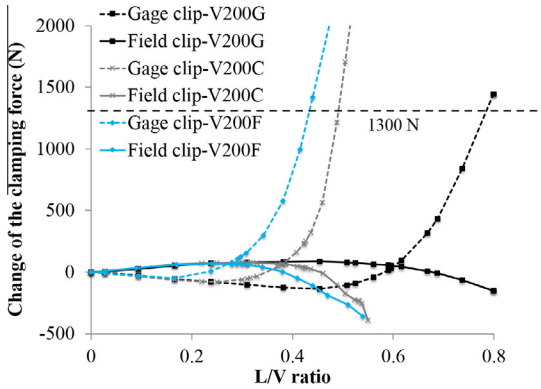

Fig. 12. Changes of the clamping force of the gage and field clips with respect to *L*/*V* ratio under various vertical loading positions.

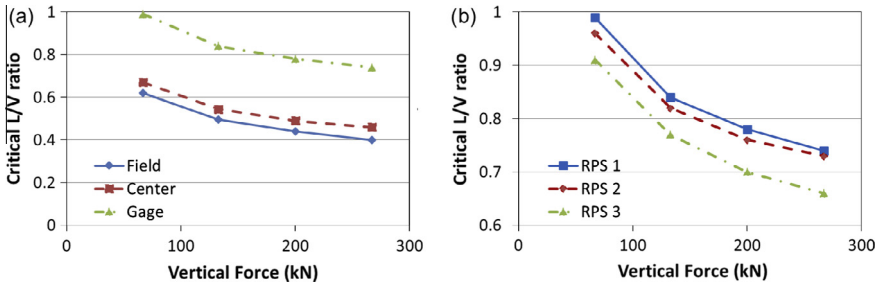

Fig. 13. Critical *L*/*V* ratio of fastening system (a) with RPS1 versus vertical load applied at various locations and (b) with different rail pad system and vertical load applied at gauge side.

field side (V200F). As shown in the figure, the critical *L*/*V* ratios where the change of clamping force started to exceed 1300 N (300 lb) criteria were found to be 0.78, 0.49, and 0.44 for V200G, V200C and V200F, respectively. Furthermore, the result demonstrated that the change rate of the clamping forces was not severe up to certain *L*/*V* ratios, and after those points, exponential changes were observed. When the vertical load was applied toward the field side on the rail head, the fastening system became more vulnerable due to extra rotation of the rail.

Fig. 13 shows the critical *L*/*V* ratios of all 12 simulations where the changes of the clamping force exceeded the 1300 N (300 lb) limit. When the *L*/*V* ratio was higher than the critical *L*/*V* ratio, yielding of the clips was observed. In general, when the vertical load was applied at the gage side, the fastening system was able to bear a higher *L*/*V* ratio because the vertical load at the gage side delayed the overturning of the rail. In other words, the vertical force applied at the field side exacerbated the fastening system due to increased moment. This study indicated that the worst scenario is observed at an *L*/*V* ratio of 0.40 when a 267 kN (60 kips) vertical load is applied at the field side. However, in normal service conditions, i.e. when the vertical load is applied at the gage side of rail head, the fastening system would be sustainable up to an *L*/*V* ratio of 0.74. However, this might not be the case should the vertical force is applied at the field side or center of the rail head due to irregularities of the track structures and defects of the wheel (e.g. hollow-worn out wheel and truck hunting).

The responses of the fastening systems with different rail-seat pads systems were also investigated in terms of the critical *L*/*V* ratio (Table 1). The cases with the vertical force at the gage side were discussed since the effects of the location of the vertical forces were described in the previous section. The critical *L*/*V* ratios are presented in Fig. 13.b for the three different pad systems. The results indicate that the softer the pads system, the smaller is the critical *L*/*V* ratio. The change of clip behavior was not so severe when the RPS 1 was replaced by the RPS 2, while the change became noticeable with the RPS 3. The critical *L*/*V* ratios when using RPS 3 was found to be 0.05–0.08 less than in the cases when RPS 1 is used. Considering all the variation of wheel load magnitude and location, and the material property of pad system in this parametric study, it can be observed that an *L*/*V* ratio of 0.4 is the threshold for possible clip yielding. In other words, for an *L*/*V* ratio less than 0.4, the rail clips will behave elastically in most cases.

4.2. Lateral load demands on shoulder

The Shoulder of the fastening system is an important component that holds the fastening system together (see Fig. 1). However, shoulders tend to be damaged due to complex interactions within the system. Most of the previous studies have

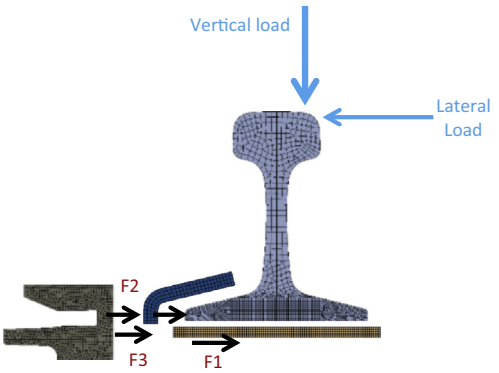

Fig. 14. Schematics of the lateral reaction forces.

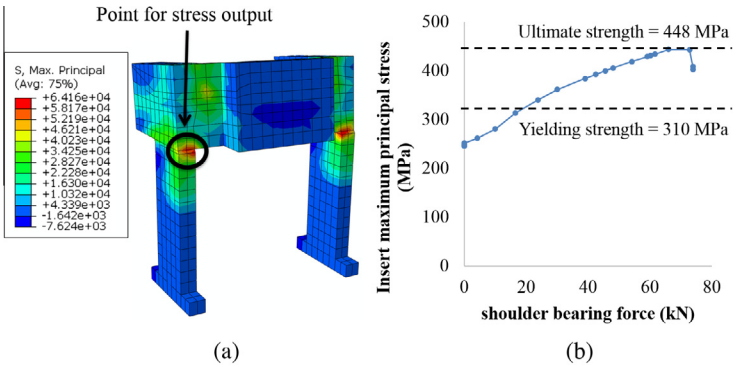

Fig. 15. (a) Maximum principal stress contour of field-side shoulder (unit: psi, 1 psi = 0.007 MPa) and (b) the relationship between shoulder bearing force and maximum principal stress when a vertical load of 267 kN (60 kips) is applied on the gauge-side rail head.

focused on identifying vertical load path within the fastening system, and due to the complexities of the system, identifying lateral load path was hindered. In this section, the lateral load path was identified with the aim of quantifying the lateral load demands on the shoulder.

Fig. 14 depicts schematics of the lateral reaction components: F1 is the lateral frictional force between rail-seat pads system and concrete crosstie, F2 is the lateral reaction force between the shoulder and insulator, and F3 is the lateral reaction force between the shoulder and the pads system. The total lateral load demand on a shoulder is the sum of F2 and F3.

Fig. 15 shows the tensile stress contour of field-side shoulder, and the change of maximum tensile stress under increasing shoulder demand (i.e. bearing force = F2 + F3), when a vertical wheel load of 267 kN (60 kips) was applied on the gage side of the rail head. Due to the reaction of clamping force, high tensile stress is observed at the bottom of shoulder inserts before the application of lateral wheel load. Under lateral load the shoulder behaves similar to a cantilever beam in flexure, as the shoulder is fixed at the shoulder inserts. As a result, the tensile stress at the joint between the shoulder and the inserts continued to increase until yielding is reached.

This failure mechanism of shoulder is directly related to the magnitude of shoulder demand, and the shoulder demand is affected by the L/V ratio, and the material property of rail pad. Fig. 16 shows the change of F1, F2, and F3 reactions with respect to L/V ratio when using pad systems RPS 1 and RPS 3. For the cases shown a vertical load of 200 kN (45 kips) was applied at the gage side. The solid line with the square marks represents the results with the RPS 1, and the dashed line with the cross marks represents the results with the RPS 3. When the L/V ratio was relatively low, most of the lateral force was resisted by the friction F1. However, the lateral load demand on the shoulder gradually increased and more than half of the lateral force was transmitted to the shoulder at higher L/V ratios. The magnitude of frictional force mainly depended upon the contact area between the concrete and the rail pad, and the contact area became very narrow under high L/V ratio due to the rotation of the rail. This trend was observed for all simulation cases. When the soft pad system (RPS 3) was used in the fastening system, one of the most noticeable changes was that the frictional force decreased, while the lateral load demand on shoulder increased. It was observed that larger portion of the lateral load was resisted by the shoulder when softer pad system was used.

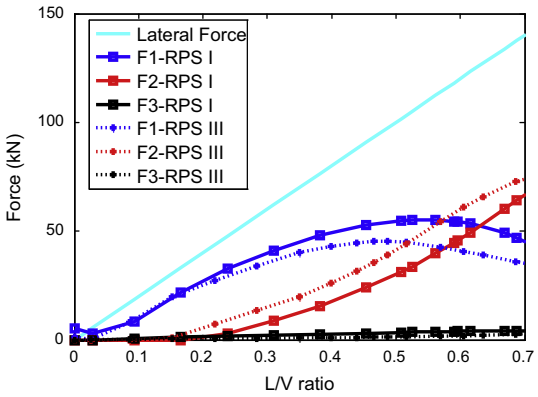

Fig. 16. Lateral loading distribution for V200G with RPS 1 and RPS 3.

5. Conclusions and recommendations

This study focused on the analysis of some critical failure mechanisms of the concrete crosstie and fastening system using a validated FE model. A detailed FE model that included one prestressed concrete crosstie and two sets of fastening system was presented and analyzed under various loading scenarios. Some important mechanisms that could affect the performance of concrete crosstie and fastening system were considered in the FE model. These mechanisms included: (1) Contact behavior at the interfaces between different model components, (2) Prestress release of the concrete crosstie and bond-slip behavior between concrete and prestressing strands, and (3) Nonlinear constitutive behavior of component materials. Parametric studies were carried out to investigate two major failure mechanisms of the concrete crosstie and fastening systems, namely the tensile cracking of the concrete crosstie and the damage of the fastening system in clip and shoulder. The following are the main conclusions of this study:

- The transfer length of prestressed concrete crossties gradually reduced with higher bond-slip stiffness between concrete and prestressing strands. For prestressed concrete crossties of similar dimensions, the threshold of reinforcement bond-slip stiffness to develop sufficient effective prestress at the rail-seat region is 16,502 MPa/m, which is the equivalent pull-out stress divided by the reinforcement end slip.
- Gaps between the concrete crosstie and ballast at the rail-seat region considerably increase the flexural demand at the crosstie center. For the crosstie type considered in this study a gap larger than 2.54 mm (0.1 in.) resulted in tensile cracking of concrete at the top surface of crosstie midspan.
- The critical L/V ratio was defined as the threshold that clip yielding was observed for higher lateral wheel load. The critical L/V ratio decreased with higher vertical wheel load. When the vertical wheel load was applied on the gage side as designed, loading scenarios of L/V ratio lower than 0.74 did not result in damage in the clips.
- Both the location of vertical wheel load and the material property of the pad system affect the critical L/V ratio of the system. Under an L/V ratio less than 0.4 the clips behaved elastically in most cases.
- Under high shoulder demand, tensile yielding is observed at the joint between the shoulder and the inserts on the field-side shoulder. The shoulder demand increased with the magnitude of lateral wheel load, and higher shoulder demand was observed with softer rail pad system.

To further investigate the wheel load path through the concrete crosstie and fastening system, static analysis was used in this study. It should be noted that based on the FE model presented in this study, further work using dynamic analysis is in progress. In addition, current FE model only captures the response of a single crosstie. In further studies the model will be improved to consider the distribution of vertical and lateral wheel load among multiple crossties in track condition.

Acknowledgements

The authors would like to express their sincere gratitude to the United States Department of Transportation (US DOT) Federal Railroad Administration (FRA) for providing funding for this research project. The published material in this paper represents the position of the authors and not necessarily that of DOT. Industry partnership and support has been provided by Union Pacific Railroad; BNSF Railway; National Railway Passenger Corporation (Amtrak); Amsted RPS/Amsted Rail, Inc.; GIC Ingeniería y Construcción; Hanson Professional Services, Inc.; and CXT Concrete Ties, Inc., an LB Foster Company. The authors also would like to acknowledge research engineer Marcus Dersch and Ryan Kernes for facilitating the communication with industrial partners.

References

[1] AREMA. Manual for Railway Engineering, Ties, AREMA, Lanham, MD 20706; 2010.
[2] González-Nicieza C, Álvarez-Fernández MI, Menéndez-Díaz A, Álvarez-Vigil AE, Ariznavarreta-Fernández F. Failure analysis of concrete sleepers in heavy haul railway tracks. Eng Fail Anal 2008;15:90–117.
[3] Rezaie F, Shiri MR, Farnam SM. Experimental and numerical studies of longitudinal crack control for pre-stressed concrete sleepers. Eng Fail Anal 2012;26:21–30.
[4] Frohling RD. Low frequency dynamic vehicle/track interaction: modelling and simulation. Vehicle Syst Dynam 1998;29:30–46.
[5] Kaewunruen S, Remennikov AM. Nonlinear transient analysis of a railway concrete sleeper in a track system. Int J Struct Stab Dyn 2008;8:505–20.
[6] Yu H, Jeong DY. Finite element modeling of railroad concrete crossties – a preliminary study, ICRE2010 – International Conference on Railway Engineering, Beijing Jiaotong University, Beijing, China; 2010.
[7] Yu H, Jeong D, Choros J, Sussmann T. Finite element modeling of prestressed concrete crosstie with ballast and subgrade support, ASME 2011 international design engineering technical conference & computers and information in engineering conference. Washington, DC, USA: ASME; 2011.
[8] Dahlberg T, Lundqvist A. Load impact on railway track due to unsupported sleepers. Proc Inst Mech Eng, Part F: J Rail Rapid Transit 2005;219:67–77.
[9] Hanna AN. Prestressed concrete ties for North-American railroads. J Prestress Concr Inst 1979;24:32–61.
[10] International Union of Railways, Leaflet 713 Design of monoblock concrete sleepers, Union Internationale Des Chemins De Fer, 16 rue Jean Rey, 75015 Paris, FRANCE; 2005.
[11] Standards Australia, Australian Standard AS 1085.14. Railway Track Material, Standards Australia International Ltd., GPO Box 5420, Sydney, NSW 2001, Australia; 2003.
[12] Federal Railroad Administration, International Concrete Crosstie and Fastening System Survey, Washington, DC 20590; 2013.
[13] Dassault Systemes Simulia Corp. ABAQUS Analysis User's Manual, Version 6.11; 2011.
[14] Chen Z, Shin M, Andrawes B. Finite element modeling of the fastening system and concrete sleepers in North America, 10th international heavy haul association conference. New Delhi, India: International Heavy Haul Association; 2013.
[15] Chen Z, Shin M, Wei S, Andrawes B, Kuchma DA. Finite element modeling and validation of the fastening systems and concrete sleepers used in North America. Proc Inst Mech Eng, Part F: J Rail Rapid Transit 2014. 0954409714529558.
[16] Huang H, Tutumluer E. Discrete element modeling for fouled railroad ballast. Constr Build Mater 2011;25:3306–12.
[17] Grasse JS. Field test program of the concrete crosstie and fastening system. Urbana, IL 61801: University of Illinois at Urbana-Champaign; 2013.
[18] Kernes RG, Edwards JR, Dersch MS, Lange DA, Barkan CPL. Investigation of the dynamic frictional properties of a concrete crosstie rail seat and pad and its effect on Rail Seat Deterioration (RSD), Transportation Research Board 91st Annual Meeting, Transportation Research Board, Washington, D.C., USA.; 2012.
[19] Yamaguchi Y. Tribology of plastic materials: their characteristics and applications to sliding components. Elsevier Science; 1990.
[20] Stachowiak G, Batchelor AW. Engineering tribology. Elsevier Science; 2013.
[21] Holste JR, Haynes M, Peterman RJ, Beck BT, Wu C-HJ. Tensioned pullout test used to investigate wire splitting propensity in concrete railroad ties, joint rail conference. Colorado Springs, CO, USA: ASME; 2014.
[22] Mitchell DW, Marzouk H. Bond characteristics of high-strength lightweight concrete. ACI Struct J 2007;104:22–9.
[23] Abrishami HH, Mitchell D. Bond characteristics of pretensioned strand. ACI Mater J 1993;90:228–35.
[24] Rose DR, Russell BW. Investigation of standardized tests to measure the bond performance of prestressing strand. PCI J 1997;42:56–80.
[25] Du MM, Su XZ, Zhao Y. Experimental study on bond behavior of ribbed bar and strand. Jianzhu Cailiao Xuebao/J Build Mater 2010;13:175–81.
[26] Murphy RL. Determining the transfer length in prestressed concrete railroad ties produced in the United States: Kansas State University; 2012.
[27] Lutch RH, Harris DK, Ahlborn TM. Prestressed concrete ties in North America. AREMA annual conference and exposition. Chicago, IL, USA: AREMA; 2009.
[28] Sawley K, Urban C, Walker R. The effect of hollow-worn wheels on vehicle stability in straight track. Wear 2005;258:1100–8.